Linear Quadratic Gaussian predictive control for the Gran Telescopio Canarias AO system: design issues and first bench results

Lucas Marquis, Caroline Kulcsár, Iciar Montilla, Henri-François Raynaud, José Marco de la Rosa, Óscar Tubío Araújo, Alastair Basden, Marcos Reyes García-Talavera

Linear Quadratic Gaussian predictive control for the Gran Telescopio Canarias AO system: design issues and first bench results

Lucas Marquis[a], Caroline Kulcsár[a], Icíar Montilla[b], Henri-François Raynaud[a], José Marco de la Rosa[b], Óscar Tubío Araújo[b], Alastair Basden[c], and Marcos Reyes García-Talavera[b]

[a]Institut d'Optique Graduate School, Laboratoire Charles Fabry - CNRS, Université Paris-Saclay, Palaiseau, France
[b]Instituto de Astrofísica de Canarias, La Laguna, Spain
[c]Durham University, United Kingdom

ABSTRACT

The Gran Telescopio Canarias (GTC) will be soon equipped with an Adaptive Optics (AO) system. The GTCAO system[1,2] is currently at the Instituto de Astrofisica de Canarias (IAC), where tests and performance assessment are ongoing. The Institut d'Optique Graduate School-Laboratoire Charles Fabry (IOGS-LCF), through a collaboration with IAC, is exploring high performance control solutions. In this proceeding, we present first bench results for such a controller, namely a Linear Quadratic Gaussian regulator (LQG). First, we briefly describe the GTCAO bench and the principle of the LQG regulator. Second, an aspect of this development is outlined, namely the wavefront sensor measurement noise variance characterization. It is conveniently based on the use of telemetry data (wavefront sensor closed-loop slopes power spectral densities and subapertures flux) allowing for an easy-to-update and best-tuned controller. Finally, on-bench performance results are presented with an LQG regulator in the line of the previous on-sky experiments with full LQG regulator,[3,4] implemented in DARC,[5] the GTCAO RTC. Comparison is performed with the integrator as baseline controller, through evaluation of the Strehl ratio from point spread functions acquired on the scientific camera, rejection transfer functions and stability margins.

Keywords: Adaptive Optics, discrete-time LQG control, asymptotic Kalman filter, measurement noise covariance, vibration filtering

1. INTRODUCTION

1.1 GTC telescope

The Gran Telescopio Canarias telescope is until now the biggest telescope in visible/infrared wavelength range. Located in La Palma (Canaries Islands, Spain), it has a segmented primary mirror (37 segments) of equivalent diameter 10.4 m. It will be equipped next year with an adaptive optics system: the GTCAO.

1.2 GTCAO

The GTCAO is a Single Conjugated AO (SCAO) system, currently in laboratory at the Instituto de Astrofisica de Canarias (IAC), where tests and performance assessment are ongoing. It is composed of those three main components:

1. Deformable mirror (DM): Cilas piezo-electric, size 21 $\times$ 21 with 373 used actuators
2. Wavefront sensor (WFS): Shack-Hartmann with OCAM2 camera (EMCCD), size 20 $\times$ 20 with 312 used subapertures
3. Real-time controller: Durham AO Real-Time Controller[5] (DARC), which embeds an LQG controller

The typical loop sampling frequencies extend from 50 Hz to 1000 Hz, corresponding respectively to NGS magnitudes of around 14 and 10 (or less).

Further author information: lucas.marquis@institutoptique.fr

1.3 GTCAO controller

The controller baseline for GTCAO is the integrator, with a tip/tilt loop separated from the higher orders loop. The core of our work is the design of a high-performance controller based on data-driven models: the LQG controller.

1.3.1 Integrator

When closing the loop with a sampling time of T_s, the calculation of an integrator command u^INT at time kT_s using the residual wavefront slopes measurement y_k is given by

$$u_k^\mathrm{INT} = u_{k-1}^\mathrm{INT} - \left(gM_\mathrm{com}y_k + g^\mathrm{TT}M_\mathrm{com}^\mathrm{TT}y_k\right) \tag{1}$$

where M_com is the DM command matrix and $M_\mathrm{com}^\mathrm{TT}$ the tip/tilt modes command matrix. The loop gains g and g^TT are optimized on the bench according to the disturbance (phase screen, vibration) and measurement noise (variance σ_w^2, depending on the NGS magnitude M_NGS and the sampling frequency F_s).

1.3.2 Linear Quadratic Gaussian controller

For the sake of simplicity, we suppose here that GTCAO has a total loop delay of exactly two frames (one for the WFS exposure time, one for WFS camera read-out, slopes and command computation and DM reshaping).

Principle Our goal is to compute the command u_{k-1} that minimizes the residual phase variance $J(u) = \mathrm{var}(\phi_k^\mathrm{res}) = \mathrm{var}(\phi_k - \phi_k^\mathrm{cor})$. The correction phase ϕ_k^cor is related to the command vector u through $\phi_k^\mathrm{cor} = Nu_{k-1}$, N being the DM influence matrix.

To design an LQG controller, we need a state space representation of the AO system (including wavefront perturbations), obtained for example in the form

$$\begin{cases} X_{k+1} = AX_k + \Gamma v_k \\ \phi_k = C_\phi X_k \\ y_k^\mathrm{OL} = CX_k + w_k \end{cases} \tag{2}$$

where X_k is the state vector at time k, A is the state matrix containing the dynamics of the perturbation model. The disturbance ϕ_k is expressed on a Zernike base and is obtained as an output thanks to the matrix operator C_ϕ. The process noise v is zero-mean, white and Gaussian with covariance matrix Σ_v insuring that ϕ has the desired Von Kármán statistics. The matrix Γ simply ensures consistency with the dimensions of the state vector X_k. The open-loop WFS measurement Y^OL is affected by a zero-mean white Gaussian measurement noise w with covariance matrix Σ_w, and C is the observation matrix that encodes the WFS operations.

The optimal control which minimizes $J(u)$ is an LQG regulator. The control takes the form

$$u_k = N^\dagger \hat{\phi}_{k+1|k} \tag{3}$$

where $\hat{\phi}_{k+1|k} = \mathrm{E}(\phi_{k+1}|\mathcal{I}_k) = C_\phi \hat{X}_{k+1|k}$ is the output of the asymptotic Kalman filter built from (2), $\mathcal{I}_k = \{y_k, y_{k-1}, ..., u_{k-1}, u_{k-2}, ...\}$ representing all available information at time k.

Kalman filter calculation The real-time part of the asymptotic Kalman filter corresponds to the equation

$$\widehat{X}_{k+1|k} = A\widehat{X}_{k|k-1} + L_\infty \left(y_k - \widehat{y}_{k|k-1}\right) \tag{4}$$

where $\widehat{y}_{k|k-1} = C\widehat{X}_{k|k-1} - M_\mathrm{int}u_{k-2}$ is the prediction of the closed-loop residual slopes, and M_int is the interaction matrix.

The prediction Kalman gain L_∞ is computed off-line:

$$L_\infty = A\Sigma_\infty C^\mathrm{T}\left(C\Sigma_\infty C^\mathrm{T} + \alpha_\mathrm{ff}\Sigma_w\right)^{-1} \tag{5}$$

with Σ_∞ the asymptotic estimation error covariance matrix and α_{ff} is a fudge factor that allows to tune the global signal-to-noise ratio. The matrix Σ_∞ is then obtained as the solution of the following discrete algebraic Riccati equation, computed off-line:

$$\Sigma_\infty = A\Sigma_\infty A^{\mathrm{T}} + \Gamma\Sigma_v\Gamma^{\mathrm{T}} - A\Sigma_\infty C^{\mathrm{T}}\left(C\Sigma_\infty C^{\mathrm{T}} + \alpha_{\text{ff}}\Sigma_w\right)^{-1} C\Sigma_\infty A^{\mathrm{T}}. \tag{6}$$

The state matrix A and state noise covariance matrix $\Gamma\Sigma_v\Gamma^{\mathrm{T}}$ embed the disturbance model. The matrix Σ_w embeds the WFS measurement noise model. We need to model the disturbance and the measurement noise faced by the AO system as efficiently as possible in terms of control performance. We focus in this paper on the computation of Σ_w, and we explain in next section how we compute it using telemetry data.

2. AO SYSTEM MODELLING FOR LQG CONTROLLER: THE MEASUREMENT NOISE COVARIANCE MATRIX

The computation of the Kalman gain through (5) and (6) calls for the definition of the measurement noise covariance matrix $\Sigma_w = \mathrm{E}\left(w_k w_k^T\right)$. As the measurement noise is supposed here to be spatially white, Σ_w is a diagonal matrix in the form $\Sigma_w = \mathrm{diag}[\sigma_w^2(i)]_{i=1,\ldots,n_{\text{s}}}$ where n_{s} is the number of slopes ($n_{\text{s}} = 624$ slopes).

In the case of GTCAO, the telescope pupil is not circular and moreover rotates with time, see figure 1.

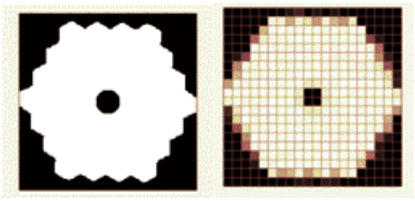

Figure 1. The non circular pupil of GTC (left) rotates with time, inducing a strongly variable flux on the WFS camera for the edges subapertures (right).

The purpose of this Section is to propose a method that computes Σ_w automatically while accounting for the flux per subaperture for a given batch of pseudo-open-loop slopes measurements. This method has been used successfully for LQG bench tests.

1. First, we need the median of the measurement noise variances of the well illuminated subapertures (that is to say subapertures with a flux level above the threshold stipulated to DARC). These are easy to pinpoint since they are delivering a non-zero measurement at every frame, so that the validity ratio is equal to 1 (never beneath the threshold). We need to have an idea of the minimal length the considered batch should have (n_{iter}) and of the bandwidth of high frequencies taken into account (n_{freq}) so as to obtain a good estimation of the noise variance from the Power Spectral Density (PSD).

   Figure 2 shows the ratios r of validation of the WFS illumination criterion according to the subaperture (left), and an example of the PSD of a y-slope for a batch size of 12000 open-loop samples recorded at 1000 Hertz (right).

   Figure 3 shows on the left the medians calculated when increasing the batch size used to compute the Power Spectral Density (PSD) and on the right when increasing the number of frequency PSD samples used for the variance calculation. In our case, either at $F_{\text{s}} = 100$ FPS or 1000 FPS, $n_{\text{iter}} = 2000$ frames and $n_{\text{freq}} = 200$ points are satisfying values as it can be seen in figure 3.

2. Secondly, we attribute a variance to the partially illuminated slopes from the estimations mentioned above. They correspond to the subapertures in which the availability ratio r (figure 2, left) is between 0 and 1 excluded. Knowing that the measurement noise variance is proportional to the light flux, we decided on the following rule:

$$\forall i \in [\![1, 624]\!], r(i) \in]0, 1[\implies \sigma_w^2(i) = \frac{1}{r(i)}\mathrm{median}\left(\{\sigma_w^2(j) | r(j) = 1\}\right). \tag{7}$$

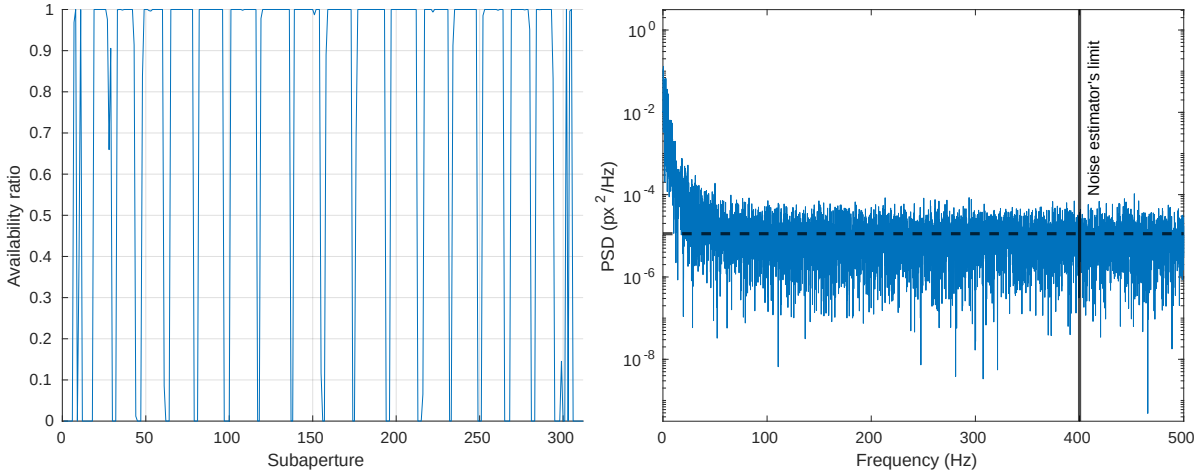

Figure 2. Left: typical ratios r of validation of the WFS illumination criteria according to the subaperture. Right: example of PSD of a y-slope (here, slope number 610/624 for a 1000-Hertz 12000-frame long OL sample), the black dashed line showing the estimated noise in $\mathrm{px}^2/\mathrm{Hz}$ as the median of the last 200 points (high frequencies 400 Hz to 500 Hz here, $n_{\mathrm{freq}} = 1200$ frequency samples): $\sigma_w^2(610) = 1.2 \times 10^{-5} \times F_{\mathrm{s}}/2 = 6.0 \times 10^{-3}$ px^2.

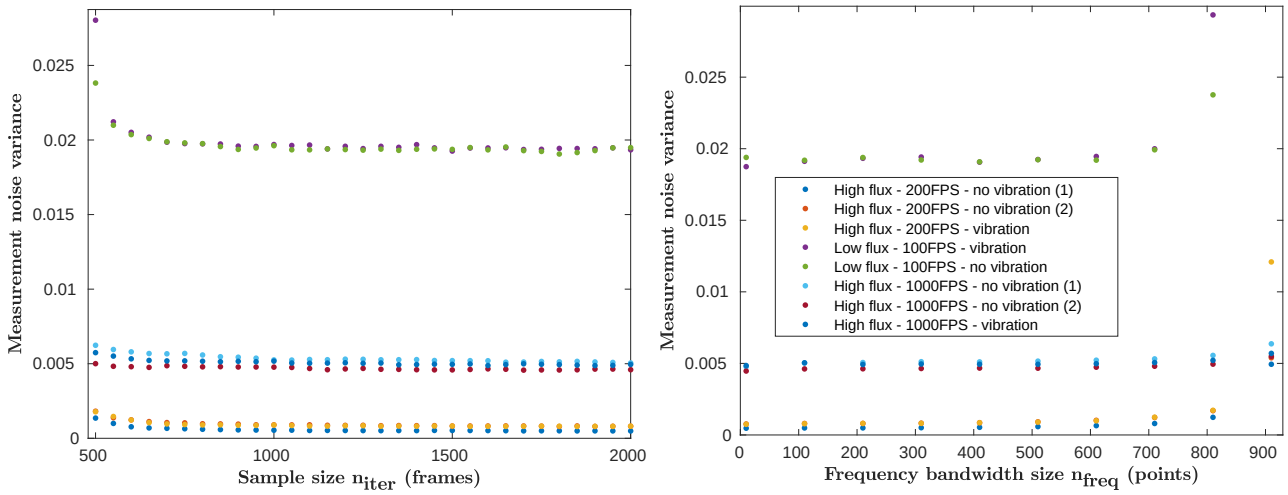

Figure 3. Slopes measurement noise variance estimations (median of the fully-illuminated slopes among the 624 obtained the same way as in figure 2). Left: for different sample sizes n_{iter}; case with $n_{\mathrm{freq}} = 200$. Right: for different numbers n_{freq} of high-frequency points; case with $n_{\mathrm{iter}} = 2000$.

3. Then, we attribute a high value $\sigma_{\mathrm{w,lim}} = c \times \mathrm{median}\left(\{\sigma_w^2(j)|r(j) > 0\}\right)$ to the never-illuminated subapertures. It needs to be extremely high since corresponding to missing measurements, but small enough to avoid numerical problems when solving the Riccati equation. Different coefficients c are leading to negligeable performance gaps when carrying out tests on the bench (those unilluminated subapertures are set to zero by DARC), allowing to take c roughly between 20 and 1000. It was decided to take $c = 100$.

Once the three steps are completed (requiring not even one second of computation on a standard laptop) we dispose of an appropriate matrix Σ_w (example in figure 4) that allows for starting the Kalman gain matrix computation.

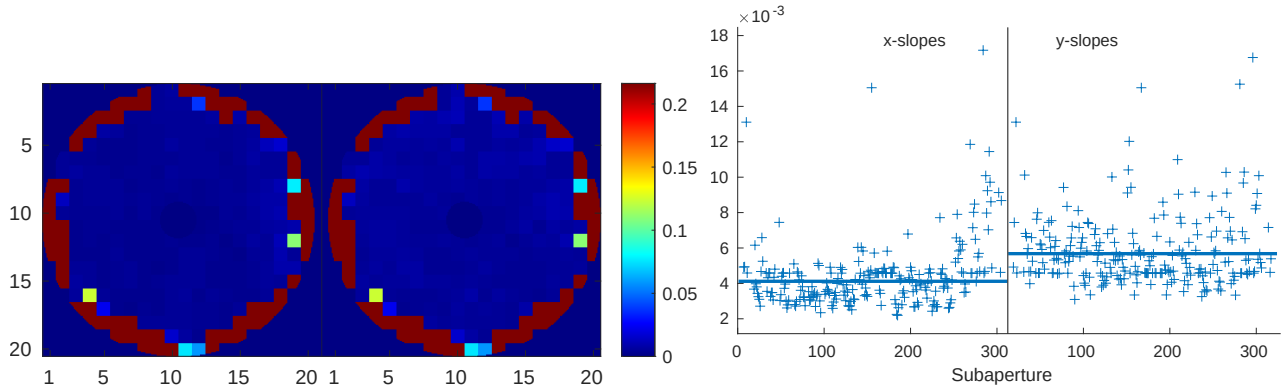

Figure 4. Slopes measurement noise variance estimations, in px^2, following the procedure described above (using a batch of slopes at high flux recorded at 1000 FPS). Left: in 2D pupil plan. Right: on a graph, unilluminated subapertures cut out, with median drawn as a horizontal blue bar. Both: x-slopes on the subleft and y-slopes on the subright

Notes For some reasons, the y-slopes clearly seem to be more subject to measurement noise than the x-slopes are (cf figure 4).

Also, it is clear that setting a high variance value for a given slope (like taking $c = 100$) roughly amounts to nullify the corresponding column in the Kalman gain L_∞ or equivalently to replace the corresponding measurement by its prediction.

3. ON-BENCH RESULTS

We present here some of the results obtained on the GTCAO bench when closing the loop with an integrator or with an LQG controller.

3.1 Bench parameters

The turbulence (rotating phase screen) corresponds to a single layer of Fried parameter $r_0 = 9\,\mathrm{cm}$ and wind speed $V_0 = 10\,\mathrm{m\,s^{-1}}$. We have also independently some windshake-induced vibrations: we introduce artificially with the DM a peak of energy in both tip and tilt PSD, at 12 Hz and of RMS 20 mas as described by the GTC mechanics team,[2] as illustrated in figure 5 with the OL tip-mode PSD.

3.2 Strehl ratios

We consider in this paper two NGS magnitude cases: first, magnitude 10.2 (with 900 FPS sampling rate) and second, magnitude 11.3 (400 FPS). All regulators have been tuned in order to get their best performance in each case (integrator tip-tilt and DM gains, and LQG fudge factor).

The LQF regulator reaches 37.5 % of Strehl Ratio (SR) for both magnitudes, while the integrator gives a value of 34.5 % SR for magnitude 10.2 and 32 % SR for magnitude 11.3. It is worth noting that despite the loop frequency decrease (from 900 FPS to 400 FPS), the LQG regulator maintains its performance at the same level thanks to its predictive capacity. Figure 6 presents the profiles associated with the four corresponding Point

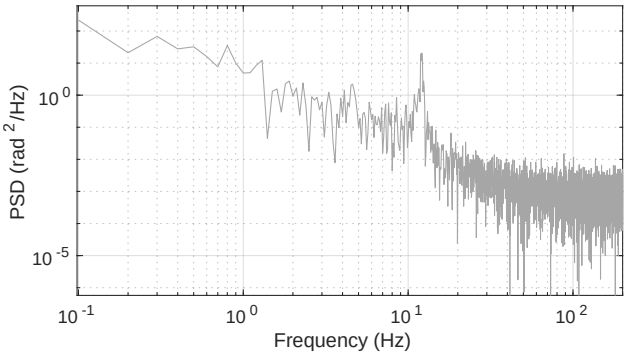

Figure 5. PSD of tip perturbations: turbulence and 12-Hz vibration (20 mas RMS).

Spread Functions (PSFs), showing the increase of the peak intensity provided by the LQG (9 % increase for magnitude 10.2 and 19 % for magnitude 11.3).

The use of the procedure presented above for the calculation of Σ_w has allowed an increase of 1.5 to 3.5 points of SR (depending on the turbulence strength, magnitude and presence of vibration where highest increases have been obtained) with respect to using a standard calculation where all measurement noise variances are deduced only from the slopes PSDs plateaus. The LQG thus allows better performances than the integrator while closing

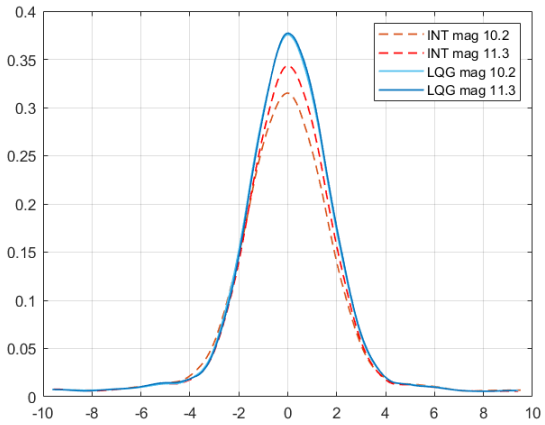

Figure 6. Profiles of the PSFs (in Airy disk peak unit) obtained with integrator and LQG regulator in two cases: magnitude 10.2 (900 FPS sampling rate) and magnitude 11.3 (400 FPS sampling rate). The x-axis is in pixels of the scientific camera.

the loop with lower sampling frequency. It allows thus to possibly decrease the WFS camera gain in order to increase the camera longevity.

3.3 Behavior

We describe hereafter some behavioral aspects for the case with magnitude 11.3 (400 FPS).

3.3.1 Rejection transfer functions

Figure 7 presents the Rejection Transfer Functions (RTFs) for the LQG regulator (top) and for the integrator (bottom). The theoretical RTFs are in good agreement with the ones calculated from the bench telemetry data. This shows that the models and calibrations are well describing the bench behaviour. It is worth noting that the tilt PSD presented in figure 5 exhibits a peak at 12 Hz that is nicely compensated by the LQG RTF shown in figure 7.

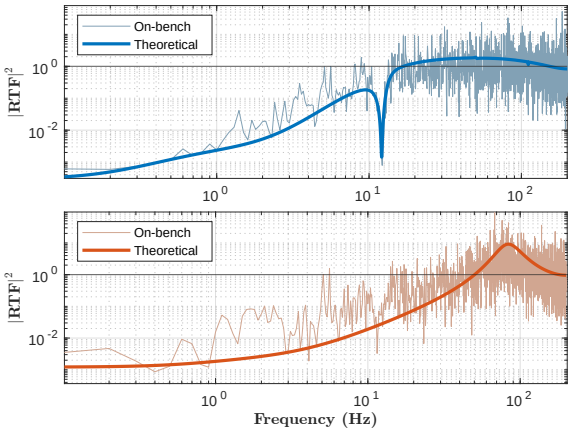

Figure 7. Rejection Transfer Functions for the LQG regulator (top) and the integrator (bottom) in the case of bad atmospheric conditions and windshake-induced vibration for magnitude 11.3. The loop rate is 400 FPS.

3.3.2 Stability and actuator solicitation

The LQG regulator has excellent stability margins, see also.[4] For the case of magnitude 11.3 (400 FPS), as shown in figure 8, the tip phase margin of the LQG is 53° and the gain margin is 13.6 dB. This is respectively around 22° and 9 dB above the integrator margins.

In addition to that, the actuators are less solicited when operating with a well-tuned LQG regulator, with on average −13 % rms of actuator stroke with respect to the integrator as shown in figure 9. Only the integrator has some commands above the DM clipping value of 3 µm.

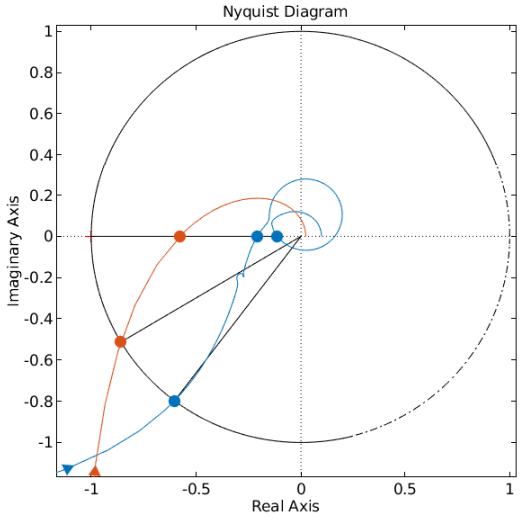

Figure 8. Tip correction Nyquist diagram for the LQG regulator (blue) and the integrator (red). The loop rate is 400 FPS.

4. CONCLUSION

In this paper, we have presented a procedure for the calculation of the measurement noise covariance matrix used in the LQG design. This procedure is fast (less than 1 s on a standard laptop), easy to update during operation

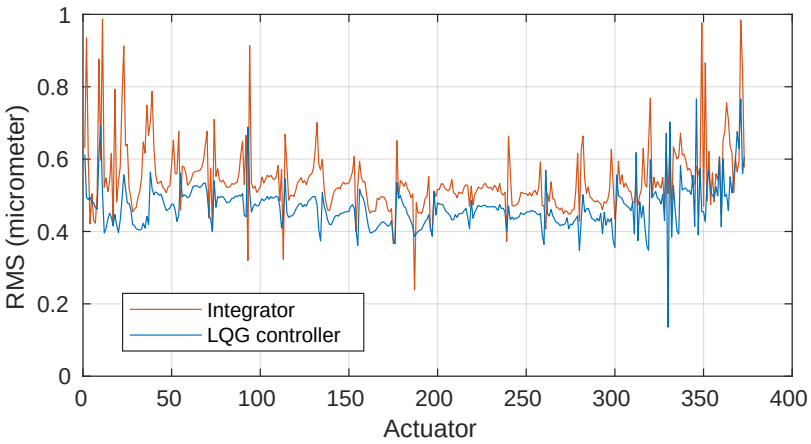

Figure 9. Example of actuators stroke temporal rms for the LQG regulator (blue) and the integrator (red).

and utilizes closed-loop measurements and a map of average flux per subaperture. It allows an increase of the Strehl ratio of 1.5 to 3.5 points depending on the observation conditions (turbulence strength, NGS magnitude, presence of vibration).

On-bench results have been presented in the case of windshake-induced vibrations and strong turbulence for two different NGS magnitudes (10.2 and 11.3). Rejection transfer functions are also displayed. The LQG regulator overpasses the integrator both in terms of SR and of stability margins.

More cases with magnitudes until 14 are left for future work, which possibly includes on-sky tests in 2023.

ACKNOWLEDGMENTS

This work is supported by the "Investissements d'Avenir" project funded by the IDEX Paris-Saclay ANR-11-IDEX-0003-02. This work has also received funding from the European Union Horizon 2020 research and innovation program, ORP Pilot, grant agreement No 101004719.

REFERENCES

[1] Bello, D., Boucher, L., Rosado, M., Castro López, J., and Feautrier, P., "Characterization of the main components of the gtcao system: 373 actuators dm and ocam2 camera," in [*Proceedings of the Third AO4ELT Conference*], 31 (2013).

[2] Cagigal, M. N., Ramosa, L. R., Araujoa, O. T., de la Rosaa, J. M., Basdenb, A., Montillaa, I., Minguell, J. R., López, R. L., Antolín, M. P., García-Talavera, M. R., et al., "Feedback control baseline for gtc adaptive optics with ngs," in [*AO4ELT5*], (2017).

[3] Sivo, G., Kulcsár, C., Conan, J.-M., Raynaud, H.-F., Éric Gendron, Basden, A., Vidal, F., Morris, T., Meimon, S., Petit, C., Gratadour, D., Martin, O., Hubert, Z., Sevin, A., Perret, D., Chemla, F., Rousset, G., Dipper, N., Talbot, G., Younger, E., Myers, R., Henry, D., Todd, S., Atkinson, D., Dickson, C., and Longmore, A., "First on-sky scao validation of full lqg control with vibration mitigation on the canary pathfinder," *Optics Express* **22**, 23565–23591 (September 2014).

[4] Sinquin, B., Prengere, L., Kulcsár, C., Raynaud, H.-F., Gendron, E., Osborn, J., Basden, A., Conan, J.-M., Bharmal, N., Bardou, L., et al., "On-sky results for adaptive optics control with data-driven models on low-order modes," *Monthly Notices of the Royal Astronomical Society* **498**(3), 3228–3240 (2020).

[5] Basden, A., Geng, D., Myers, R., and Younger, E., "Durham adaptive optics real-time controller," *Applied Optics* **49**, 6354–6363 (Nov. 2010).